Generation of frequency tunable polarization entangled photon pairs

Atsushi Yabushita and Takayoshi Kobayashi

Citation: Journal of Applied Physics **99**, 063101 (2006); doi: 10.1063/1.2183355
View online: http://dx.doi.org/10.1063/1.2183355
View Table of Contents: http://scitation.aip.org/content/aip/journal/jap/99/6?ver=pdfcov
Published by the AIP Publishing

Generation of frequency tunable polarization entangled photon pairs

Atsushi Yabushita[a)]
Department of Physics, Graduate School of Science, University of Tokyo, 7-3-1 Hongo, Bunkyo, Tokyo, 113-0033, Japan

Takayoshi Kobayashi
Department of Physics, Graduate School of Science, University of Tokyo, 7-3-1 Hongo, Bunkyo, Tokyo, 113-0033, Japan; Institute of Laser Engineering, Osaka University, 2-6 Yamada-oka, Suita, Osaka, 565-0971, Japan; and Department of Electrophysics, National Chiao Tung University, Hsinchu 300, Taiwan

(Received 30 March 2005; accepted 7 February 2006; published online 23 March 2006)

Photon pairs with correlated frequencies from an optical parametric system were generated by a continuous wave pump focused on a type-II nonlinear crystal with polarization entanglement. The polarization entanglement of the frequency resolved photons was measured under several typical configurations. By optimizing a condition, the degree of polarization entanglement was improved substantially. We proposed the application of the system, which can be used as a light source of wavelength division multiplexing quantum key distribution, optimizing the configuration of the photon-pair generation. © *2006 American Institute of Physics*. [DOI: 10.1063/1.2183355]

INTRODUCTION

Photon pairs generated by the spontaneous parametric down conversion (SPDC) in a nonlinear crystal can be entangled in various parameters. The polarization entanglement of these SPDC photon pairs has been utilized in varieties of quantum information experiments to demonstrate quantum teleportation, quantum key distribution, and others.[1]

The wave vector entanglement has also been used in various experiments, as quantum imaging,[2,3] photonic de Broglie wavelength measurement,[4–6] quantum interference,[7,8] and quantum lithography.[9–11]

Photon pairs correlated in their frequencies were used for nonlocal pulse shaping[12] and spectroscopy.[13] In Ref. 13, signal and idler photons of SPDC photon pairs were separated from each other by a polarizing beam splitter, which destroys the polarization entanglement. There are two methods which can separate the photon pairs maintaining their polarization entanglement.

The first method is as follows. The emission angles of the signal and idler photons can be tuned by rotating the nonlinear crystal around the vertical axis transversing the incident point of the pump beam.[14] When the angle of the nonlinear crystal θ_1 was set to overlap the idler and signal light cones [Fig. 1(a)], the photon pairs are in a polarization entangled state selecting photon pairs emitted into the overlapping sections, which were separated from each other. Selecting the overlapping sections, the separated polarization entangled photon pairs can be obtained.

The second method is as follows. When the angle of the nonlinear crystal θ_2 was set to touch the idler and signal light cones [Fig. 1(b)], the photon pairs are in a polarization entangled state selecting photons traveling collinearly in the pump-beam direction. Using a nonpolarizing beam splitter, the photon pairs can be separated maintaining their frequency correlation. The required condition to be satisfied by the system to perform the experiment is quite similar to our previous experimental system,[13] which makes its implementation much easier than that of the first method. This is the reason of the second method adopted in the present work.

The obtained photon pairs are entangled in polarization even after they are resolved by their frequency, therefore they can be used as a source of wavelength division multiplexing quantum key distribution (WDM-QKD). A scheme for quantum key distribution is also shown in Ref. 15.

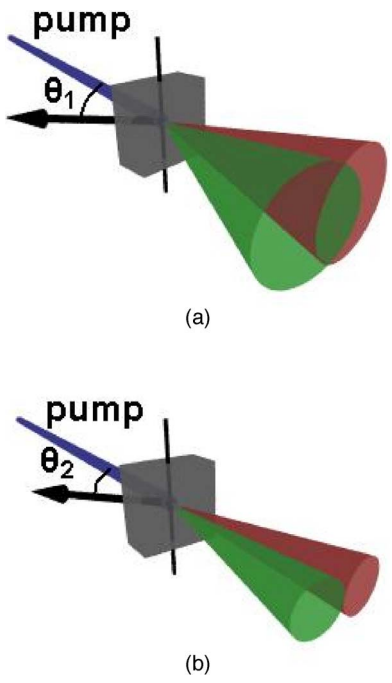

FIG. 1. (Color online) (a) and (b) show the SPDC light cones, when they overlap and touch, respectively. Arrows show the optical axis of the nonlinear crystal.

[a)]Electronic mail: yab@femto.phys.s.u-tokyo.ac.jp

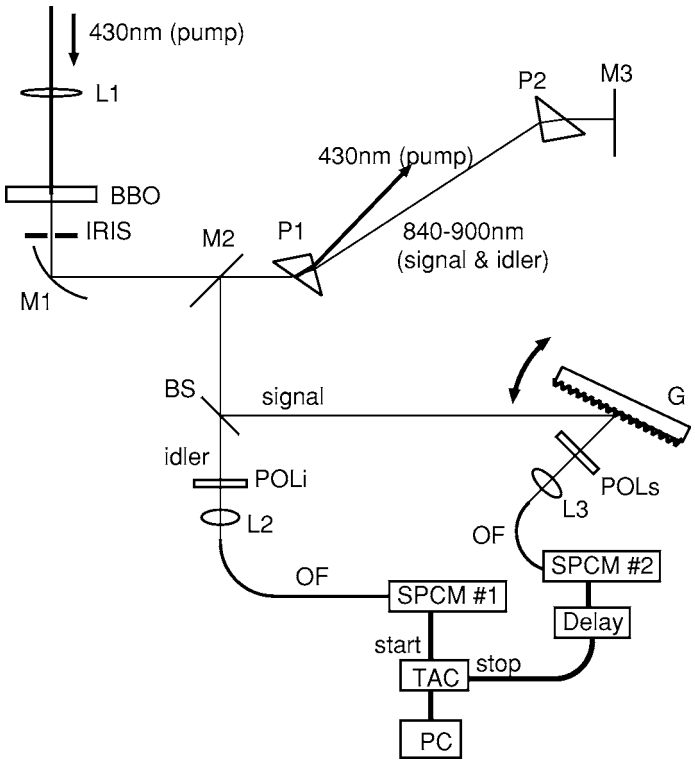

FIG. 2. Experimental setup.

In this article, we have generated the frequency resolved polarization entangled photon pairs by a small modification of our previous experimental system.

EXPERIMENT

The schematic drawing of our experimental setup is shown in Fig. 2. Frequency-nondegenerate photon pairs were generated by SPDC in a 1-mm-thick type-II β-BaB_2O_4 (BBO) crystal pumped by the second harmonic (1.5 mW) of a cw Ti:sapphire laser operated at 859.4 nm. Signal and idler photons of the SPDC pairs were emitted conically from the focal waist where the pump light was focused on the BBO crystal by a lens of 1000 mm focal length ($L1$). An iris (IRIS) was placed 100 mm behind the BBO crystal and clipped the contact point between the signal and idler light cones, where the SPDC photon pairs were entangled. The photon pairs were transmitted through the iris and collimated by an off-axis parabolic mirror (M) of 25.4 mm focal length. A prism ($P1$) was used to eliminate the remainder of the pump light, which can be a noise source in the experiments. The numbers of SPDC photon pairs are much less than that of the pump light, therefore the latter must be completely eliminated by spatial separation, and the photon pairs should travel a long path until lateral separation becomes large enough. In contrast, the elongation of the path length increases the angular dispersion of the photon pairs concomitantly with increasing spectral width. Another prism ($P2$) was used to compensate angular dispersion induced by the prism $P1$. When the light beam passes through the prism pairs, the beam height was slightly lowered by a mirror ($M3$), and the SPDC pairs were picked out by another mirror ($M2$). The signal and idler photons were separated from each other by a nonpolarizing beam splitter (BS). A linear polarizer (POL_i) was placed in the path of idler photons which transmit BS. The polarizer was on a motor driven rotation stage, and its angle was computer controlled. Signal photons (photons reflected by the BS) were diffracted by a grating (G) (1400 grooves/mm). In the signal light path, we placed another linear polarizer (POL_s), whose angle was also computer controlled.

THEORY

Each SPDC photon pair generated by the type-II BBO crystal consists of a horizontally polarized photon and a vertically polarized photon. In the present work, we considered the state whose density matrix is defined as follows:

$$\hat{\rho} = \left(\frac{1}{2}+\delta\right)|H\rangle_s\langle H|_s \otimes |V\rangle_i\langle V|_i + \left(\frac{1}{2}-\delta\right)|V\rangle_s\langle V|_s \otimes |H\rangle_i\langle H|_i + \sqrt{\frac{1}{4}-\delta^2} f e^{-i\alpha}|H\rangle_s\langle V|_s \otimes |V\rangle_i\langle H|_i + \sqrt{\frac{1}{4}-\delta^2} f e^{i\alpha}|V\rangle_s\langle H|_s \otimes |H\rangle_i\langle V|_i, \quad (1)$$

where $|H\rangle_j$ and $|V\rangle_j$ are single-photon states with horizontal and vertical polarizations, respectively. The suffixes $j=s$ and i correspond to the states of a signal and an idler photon, respectively. Here, $f(0\leqslant f\leqslant 1)$ is a parameter which indicates the purity of the state. When $f=0$, the pair is in a fully classical mixed state. When $f=1$, the state is a pure state. Under the additional condition of δ and $\alpha=0°$, 180°, the state becomes one of the maximally entangled states, known as the Bell states.

The coincident counting rate of the photon transmitted through the polarizer POL_i and through the polarizer POL_s is given by

$$n(\theta_s,\theta_i) = \mathcal{N}\left\{\left(\frac{1}{2}+\delta\right)\sin^2\theta_s\cos^2\theta_i + \left(\frac{1}{2}-\delta\right)\cos^2\theta_s\sin^2\theta_i + \sqrt{\frac{1}{4}-\delta^2}\frac{f\cos\alpha}{2}\sin 2\theta_s\sin 2\theta_i\right\}, \quad (2)$$

where θ_j is the angle between the polarizer axis and the vertical axis. Suffixes $j=s$ and i represent the polarizer POL_s and POL_i, respectively. Here $\mathcal{N}$ is a proportionality constant which can be determined from the experimental condition.

In this article, $\Theta_i(\theta_s)$ is defined as the angle θ_i at which the coincidence counting rate is maximized when θ_i is varied. When the state is one of the four Bell states $|H\rangle_s|V\rangle_i + |V\rangle_s|H\rangle_i$, i.e., $f=1$, $\delta=0$, and $\alpha=0°$, Eq. (2) gives $n(45°)=(\mathcal{N}/4)(1+\sin 2\theta_i)$, $n(135°)=(\mathcal{N}/4)(1-\sin 2\theta_i)$, and $n(0°)=(\mathcal{N}/2)\sin^2\theta_i$. Therefore, $\Theta_i(45°)=45°$ and $\Theta_i(135°)=-45°$ are rotated by 45° anticlockwise and clockwise, respectively, from $\Theta_i(0°)=90°$.

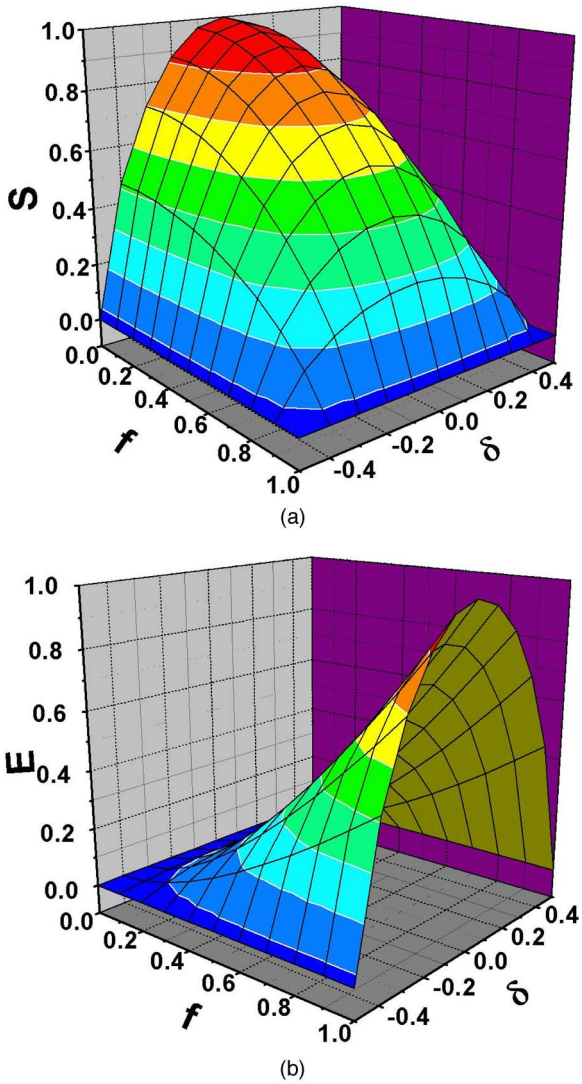

FIG. 3. (Color online) (a) and (b) are the calculated results of the von Neumann entropy, S, and the entanglement of formation, E, respectively, of the state $\hat{\rho}$ with various parameter sets of f and δ.

The von Neumann entropy, which is a measure of the purity of a quantum state $\hat{\rho}$, is defined by[16]

$$\mathcal{S} = -\operatorname{Tr} \hat{\rho} \log_2(\hat{\rho}) = -\sum_x \lambda_x \log_2 \lambda_x, \tag{3}$$

where $\{\lambda_x\}$ is a set of eigenvalues of $\hat{\rho}$. The state of Eq. (1) has two nonzero eigenvalues expressed as

$$\lambda_1 = \frac{1}{2} + \sqrt{\frac{f^2}{4} - \delta^2 f^2 + \delta^2},$$

$$\lambda_2 = \frac{1}{2} - \sqrt{\frac{f^2}{4} - \delta^2 f^2 + \delta^2}. \tag{4}$$

Using Eqs. (3) and (4), the von Neumann entropy of the state was calculated [see Fig. 3(a)].

The concurrence, entanglement of formation, and tangle are the three often used measures of quantum coherence properties of a mixed quantum state.[17,18] The concurrence C of the state $\hat{\rho}$ can be calculated as[19]

$$C = 2\left| \sqrt{\frac{1}{4} - \delta^2} f e^{-i\alpha} \right|. \tag{5}$$

The tangle is given by $T = C^2$ and the entanglement of formation by[20]

$$E = h\left(\frac{1 + \sqrt{1 - C^2}}{2} \right), \tag{6}$$

where $h(x) = -x \log_2 x - (1-x)\log_2(1-x)$. The entanglement measures of formation were calculated using Eqs. (5) and (6), and the results are shown in Fig. 3(b).

RESULTS AND DISCUSSION

At first, the detector of signal photons was set in the zeroth-order diffraction from the grating. Real signals used in the latter discussion was obtained by the detector set in the first-order diffraction. The polarization correlation of the SPDC photon pairs was measured by setting the diameter of the iris ϕ to be 12 or 1 mm (see Fig. 4). The coincidence counts were measured by rotating the angle of the polarizer (POL_i) for several angles (0°, 45°, 90°, and 135°) of the polarizer (POL_s). The zero degree of the angle was defined by an arbitrary origin of the motorized continuous rotation stage, on which the polarizer was fixed. When the angle was zero degree, the polarizer axis was nearly parallel to the vertical axis. The counted data were fitted to Eq. (2), with fitting parameters of $\mathcal{N}$, δ, and $f \cos \alpha$ (see Table I).

Figure 4 shows that the SPDC photon pairs were entangled when the diameter of the iris was 1 mm, but not entangled in the case when the diameter was 12 mm. It can be quantitatively shown from the fitted results listed in Table I as follows. The fitted result shows that the smaller iris makes $f \cos \alpha$ larger.

When the linearly polarized photons get a finite ellipticity in the experimental setup, which is mainly caused by the grating, the value of α will be modified corresponding to the amount of the ellipticity. The ellipticity was measured to be less than 0.03 using a collimated white light source, which was linearly polarized using a polarizer. Therefore the variation of α was neglected in the present analysis.

α is also dependent on the phase shift between the signal and idler photons caused by the birefringence of the BBO crystal. The path lengths of the photon pairs in the BBO crystal were calculated when the pairs are transmitting through the center of the iris and the edge of the iris. The difference of the path lengths is nearly proportional to the square of the angle between the two light paths which are passing through the center of the iris and the edge of the iris. The path length difference causes 0.2 nm of the phase shift when the iris diameter was set at 1 mm. When the iris diameter was set at 12 mm, the phase shift was calculated as 10 nm. We took into account the fact that the fiber coupler used in the present setup can collect a beam of which diameter is less than 6 mm. The phase shifts of 0.2 and 10 nm are much smaller than the center wavelength of the SPDC photons, 866 nm. Therefore α can be assumed to be same independent of the iris diameter. It means that the value of f was largely modified when the diameter of the iris was changed.

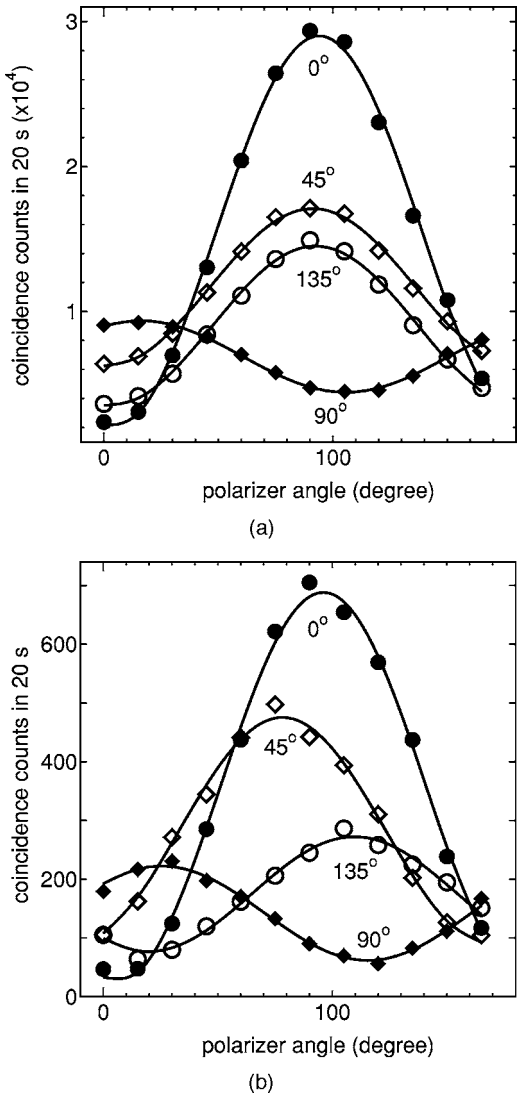

FIG. 4. Measured coincidence counts of polarization correlated photon pairs. Marks in the figure show the results measured by rotating the angle of the polarizer POL_s, when the polarizer POL_i was fixed to 0° (filled circle), 45° (open circle), 90° (filled diamond), and 135° (open diamond), respectively. The diameter of the iris was (a) 12 mm and (b) 1 mm. Curves show the results fitted by a function of Eq. (2).

The reason of the variation is as follows. If the diameter of the iris is increased, the spacial mode overlap becomes smaller, which degrades the purity of the state and reduce f. Figure 3(b) shows that when $\delta \neq \pm\frac{1}{2}$ the entanglement of formation increases with f. It means that SPDC photon pairs were entangled by spatially selecting the contact point between the signal light cone and the idler light cone (Fig. 1).

For each SPDC photon pair, the sum of the frequencies of the signal and idler photon is equal to the pump frequency. The spectral width of the pump laser (<MHz) is negligibly small compared to the spectral width of the SPDC photon pair (>THz), because the continuous laser was used as the pump. That is to say the frequencies of the signal and idler photons are strongly correlated. The frequency combinations of the signal and idler photon have variety in their spectral regions. As shown in Fig. 2, any frequency combination of frequency correlated photon pairs can be picked out by controlling the grating angle so that the first-order diffraction light from the grating was pointed to the detector of signal photons. Therefore the frequency combination of the photon pairs is tunable in our setup.

TABLE I. Results of the fitting when the detector of signal photons was positioned in the zeroth-order diffraction directions from the grating.

ϕ	δ	$f\cos\alpha$
12 mm	0.32±0.02	0.029±0.06
1 mm	0.32±0.02	0.58±0.07

Signal wavelength dependence of the coincidence counting rate of $|H\rangle_s|V\rangle_i$ was measured by rotating the grating around the vertical axis transversing the incident point of the signal beam. The angles of the polarization axes of POL_i and POL_s were adjusted to the vertical and horizontal directions for idler and signal, respectively. Then, signal wavelength dependence of the coincidence counting rate of $|V\rangle_s|H\rangle_i$ was also measured in the same way as $|H\rangle_s|V\rangle_i$.

The results of signal wavelength dependence shown in Fig. 5(a) demonstrate that the coincidence counting rate of $|H\rangle_s|V\rangle_i$ was about three times higher than that of $|V\rangle_s|H\rangle_i$ when the signal wavelength was 866 nm, and both rates were nearly balanced when the signal wavelength was 870 nm. The differences in intensity and spectral position and shape are due to the slightly unbalanced transmittance/reflectance of the real beam splitter and the diffraction efficiency of the grating have polarization dependency in the real experimental setup used in the present study.

By using a ray tracing method under phase matching condition we have numerically simulated the spectra of $|H\rangle_s|V\rangle_i$ and $|V\rangle_s|H\rangle_i$, of which result is shown in Fig. 5(b). The polarization dependency of the diffraction efficiency of the grating was measured using a collimated white light source and used for the calculation of the spectrum of the photon pairs. Unbalanced transmittance/reflectance of the real beam splitter was also taken into account in the calculation. The result of the numerical simulation fits well with the measured result, which shows that the unbalance of the polarization is caused by the optical components. Figure 5(c) shows the result of the numerical simulation when the optical components do not have any polarization dependence, and the polarization is balanced in all of the spectrum width. The full width at half maximum (FWHM) of the spectrum is 6 THz. In the telecom wavelength region, the typical frequency interval of the frequencies in the WDM communication is about 50 GHz, therefore bandwidth of 6 THz enables WDM communications in 120 channels.

Under the two typical sets of frequency combinations, the polarization entanglement of the photon pairs was measured as follows.

First, the grating angle was set to diffract 866 nm signal photons to the detector, and the diameter of the iris was set to be 1 mm. Figure 6(a) shows the measured polarization correlation of the SPDC photon pairs in this case. The counted data were fitted by the function of Eq. (2), with fitting parameters of $\mathcal{N}$, δ, and $f\cos\alpha$ (see Table II).

The experimental result of $\Theta_i(45°)$ and $\Theta_i(135°)$ being shifted from $\Theta_i(0°)$ by $10°(<45°)$ indicates that even

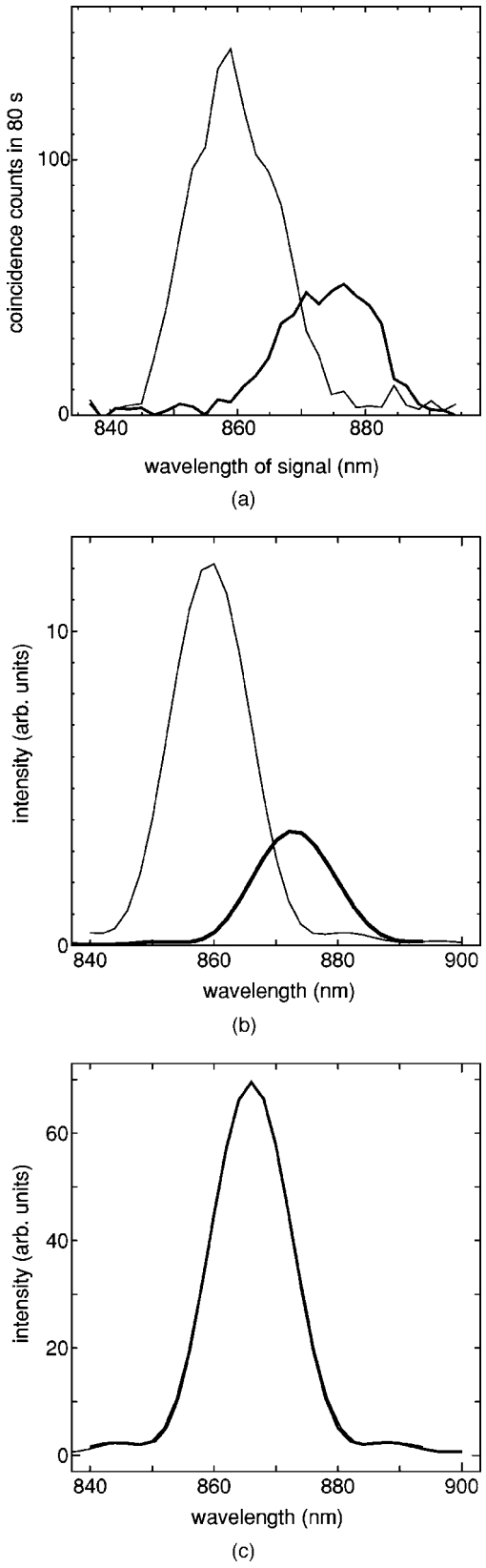

FIG. 5. Signal wavelength dependence of the coincidence counts of $|H\rangle_s|V\rangle_i$ (thick curves) and $|V\rangle_s|H\rangle_i$ (thin curves). (a) shows the result of the measurement. (b) and (c) show the results of the numerical simulations calculated with the real experimental parameters and the ideal experimental parameters, respectively. In the case of (c) both curves are almost completely overlapping with each other.

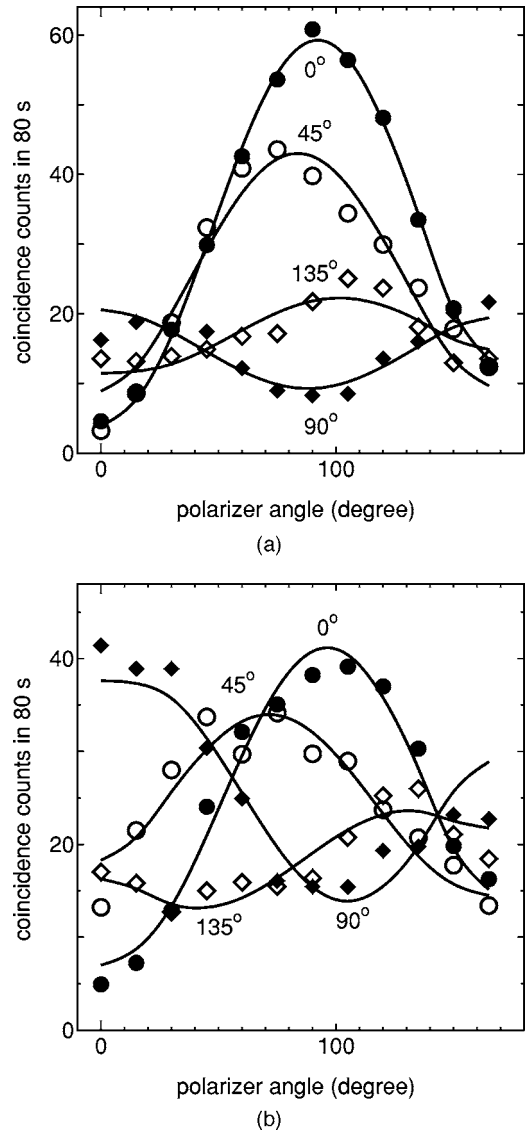

FIG. 6. [(a) and (b)] Measured coincidence counts of polarization correlated photon pairs when the coincidence counts of $|H\rangle_s|V\rangle_i$ and $|V\rangle_s|H\rangle_i$ were unbalanced (balanced with a 870 nm signal). Marks in the figures show the results measured by rotating the angle of the polarizer POL_s, when the polarizer POL_i was fixed at 0° (filled circles), 45° (open circles), 90° (filled diamonds), and 135° (open diamonds). Curves show the results fitted with Eq. (2) with the parameter set in Table II.

though the SPDC photon pairs were entangled they were not maximally correlated. It can be quantitatively shown by the fitted result in the upper row of Table II as follows. Figure 3(b) represents the following two features. First, when $f=0$ or $\delta=\pm 0.5$, the entangle of formation is zero and the state

TABLE II. Fitting parameters for the curves of coincidence counts against signal polarization shown in Fig. 6 (870 nm, bottom) and those corresponding to 866 nm signal (top) when the detector of signal photons was pointed to the first-order diffraction from the grating. Upper and lower rows show the results when the wavelength of the diffracted signal λ_s are 866 and 870 nm, respectively.

λ_s	δ	$f\cos\alpha$
866 nm	0.28±0.03	0.21±0.05
870 nm	0.07±0.03	0.46±0.07

has no entanglement. Second, when the state is maximally entangled, f and δ must be unity and zero, respectively. The fitted results in the upper row of Table II show that f is substantially deviated from zero and $\delta=0.28$ indicating that the state is entangled, but not maximally.

The validity of the fitted results can be confirmed as follows. Equation (2) gives the ratio $n(90°,0°)/n(0°,90°)$ as follows:

$$n(90°,0°)/n(0°,90°)=\left(\frac{1}{2}+\delta\right)\Big/\left(\frac{1}{2}-\delta\right). \tag{7}$$

Figure 5(a) shows that the ratio was 2.9 ± 0.3 in the case when an 866 nm signal was detected, and Eq. (7) gives $\delta=0.24\pm0.02$. The value is consistent with the fitted results shown in the upper row of Table II, providing another support of the fitting.

Second, the grating angle was set to direct an 870 nm signal to the detector, and the diameter of the iris was set to be same as the first case, 1 mm. Figure 6(b) shows the measured result of the polarization correlation. The shift of Θ_i was larger than the case of an 866 nm signal because of $\delta \ll 1$. Actually, the coincidence counting rate of $|H\rangle_s|V\rangle_i$ was nearly equal to the rate of $|V\rangle_s|H\rangle_i$ [see Fig. 5(a)]. The counted data were fitted by Eq. (2), with fitting parameters of $\mathcal{N}$, δ, and $f\cos\alpha$ listed in Table II.

The shift of Θ_i increased from about 10° to 30°, indicating that the polarization entanglement was improved. The fitted results in Table II give its quantitative analysis as follows. A birefringence of the nonlinear crystal used for SPDC causes a delay between the vertically and horizontally polarized photon in each SPDC photon pair, which is the main origin of the phase difference α. The difference of the delay between the two cases in Table II can be calculated using a dispersion relations in.[21] The calculated result was 3 nm, which is negligibly small compared to the wavelength of SPDC light. Therefore, α can be safely regarded to be common to both cases in Table II.

Table II shows that δ is smaller and f is larger when the wavelength of the diffracted signal λ_s is 870 nm, compared to the case when λ_s is 866 nm. Figure 3(b) shows that smaller δ or larger f results in larger entangle of formation. Therefore, changing λ_s from 866 to 870 nm, polarization entanglement of the pair increases.

The measured results in Fig. 5(a) shows that the ratio $n(0°,90°)/n(90°,0°)$ is 1.0 ± 0.2 when 870 nm signal photons are detected, and Eq. (7) gives $\delta=0\pm0.04$. The value is consistent with the fitted results (see the lower row of Table II). It confirms the validity of the fitted results.

The experimental results show that the system successfully generated frequency correlated polarization entangled photon pairs. The photon pairs are applicable to WDM-QKD, when their qualities are improved. For the real implementation of the WDM-QKD, the following three requirements must be fulfilled.

First requirement is that the bandwidth of photon pairs must be broad and have a good frequency correlations. The generation of the broadband frequency correlated photon pairs has been successful in our previous work,[13] in which the experimental setup was nearly the same as the present one. It assures that photon pairs are frequency correlated also in the present work.

Second one is that the photon pairs must be entangled in polarization. It has been accomplished in the present work. To increase the information transfer rate and security of QKD, the polarization entanglement is expected to be improved. The improvement can be achieved by removing the walk-off and group velocity dispersion by compensation in the nonlinear crystal. The improvement can be performed by inserting a half-wave plate and a nonlinear crystal of which thickness is half of the crystal used to generate SPDC photon pairs.[22]

Third point is that the coincidence counts of $|H\rangle_s|V\rangle_i$ and $|V\rangle_s|H\rangle_i$ must be balanced in the whole spectral range of the SPDC photon pairs with the same spectrum. It can be accomplished by using optical components whose efficiencies have no polarization dependency. Actually, the transmittance/reflectance of the beam splitter and the diffraction efficiency of the grating have polarization dependency in the present study, resulting in the unbalanced coincidence counts of $|H\rangle_s|V\rangle_i$ and $|V\rangle_s|H\rangle_i$.

After the above improvement, the SPDC photon pairs will be performed in the implementation of WDM-QKD. The throughput of QKD is mainly limited by the fiber losses and detector noise (dark counts), which will be further improved by advancing technology in the future. Another method for the improvement is the WDM-QKD which can be performed using the existing techniques. In the WDM-QKD, the photon pairs are frequency resolved by Alice and Bob, and QKD will be simultaneously performed using the detectors and modulators on each frequency correlated pairs. It will linearly improve the throughput, because each spectral channel in WDM-QKD can send the same amount of information to be transferred by the normal QKD method using nonfrequency entangled photon pairs.

As a further improvement, we can use polarization entangled photon pairs of telecom wavelength,[23] which has low-loss fiber transmission. It is also recommended to use photon detectors which have low dark count probability and high detection efficiency at telecom wavelength.[24,25]

CONCLUSION

SPDC photon pairs were generated by a type-II nonlinear crystal. When we selected photons passing through the crossing point of the signal light cone and the idler light cone, the SPDC photon pairs were entangled in polarization.

The frequencies of the signal and idler photons were exactly correlated using continuous wave laser as a pump. The frequency combination sets of the photon pairs covered a broad spectral range, and the combination was tuned by simply rotating the grating angle.

The spectra of the signal and idler photons were measured by coincidence counts of the photon pairs. Selecting two typical frequency combinations of signal and idler photon, the polarization entanglement was measured. The result showed that the entanglement of formation has increased

when the coincidence counts of $|H\rangle_s|V\rangle_i$ and $|V\rangle_s|H\rangle_i$ were balanced, compared with the case when they were unbalanced.

Requirements for the real applications of WDM-QKD were also discussed. The frequency correlated polarization entangled photon pairs can be used as a source of WDM-QKD with a small change in the experimental setup.

ACKNOWLEDGMENTS

The authors would like to thank Dr. Haibo Wang, Dr. Yongmin Li and Tomoyuki Horikiri for their valuable discussion.

[1]W. Tittel and G. Weihs, Quantum Inf. Comput. **1**, 3 (2001) and references therein.
[2]Y. H. Shih, J. Mod. Opt. **49**, 2275 (2002).
[3]T. B. Pittman, Y. H. Shih, D. V. Strekalov, and A. V. Sergienko, Phys. Rev. A **52**, R3429 (1995).
[4]E. J. S. Fonseca, C. H. Monken, and S. Pádua, Phys. Rev. Lett. **82**, 2868 (1999).
[5]J. Jacobson, G. Björk, I. Chuang, and Y. Yamamoto, Phys. Rev. Lett. **74**, 4835 (1995).
[6]K. Edamatsu, R. Shimizu, and T. Itoh, Phys. Rev. Lett. **89**, 213601 (2002).
[7]D. V. Strekalov, A. V. Sergienko, D. N. Klyshko, and Y. H. Shih, Phys. Rev. Lett. **74**, 3600 (1995).
[8]C. K. Hong, Z. Y. Ou, and L. Mandel, Phys. Rev. Lett. **59**, 2044 (1987).
[9]M. D'Angelo, M. V. Chekhova, and Y. H. Shih, Phys. Rev. Lett. **87**, 013602 (2001).
[10]R. Shimizu, K. Edamatsu, and T. Itoh, Phys. Rev. A **67**, 041805 (2003).
[11]A. N. Boto, P. Kok, D. S. Abrams, S. L. Braunstein, C. P. Williams, and J. P. Dowling, Phys. Rev. Lett. **85**, 2733 (2000).
[12]M. Bellini, F. Marin, S. Viciani, A. Zavatta, and F. T. Arecchi, Phys. Rev. Lett. **90**, 043602 (2003).
[13]A. Yabushita and T. Kobayashi, Phys. Rev. A **69**, 013806 (2004).
[14]S. Takeuchi, Opt. Lett. **26**, 843 (2001).
[15]B.-S. Shi, Y.-K. Jiang, and G.-C. Guo, Appl. Phys. B: Lasers Opt. **70**, 415 (2000).
[16]M. A. Nielsen and I. L. Chuang, *Quantum Computation and Quantum Information* (Cambridge University Press, Cambridge, 2000), Chap. 11.
[17]W. K. Wootters, Phys. Rev. Lett. **80**, 2245 (1998).
[18]V. Coffman, J. Kundu, and W. K. Wootters, Phys. Rev. A **61**, 052306 (2000).
[19]K. M. O'Connor and W. K. Wootters, Phys. Rev. A **63**, 052302 (2001).
[20]D. F. V. James, P. G. Kwiat, W. J. Munro, and A. G. White, Phys. Rev. A **64**, 052312 (2001).
[21]V. Dmitriev, G. Gurzadyan, and D. Nikogosyan, *Handbook of Nonlinear Optical Crystals*, 3rd ed. (Springer, Berlin, 1999).
[22]P. G. Kwiat, K. Mattle, H. Weinfurter, A. Zeilinger, A. V. Sergienko, and Y. Shih, Phys. Rev. Lett. **75**, 4337 (1995).
[23]A. Yoshizawa and H. Tsuchida, Appl. Phys. Lett. **85**, 2457 (2004).
[24]A. Tomita and K. Nakamura, Opt. Lett. **27**, 1827 (2002).
[25]A. Yoshizawa, R. Kaji, and H. Tsuchida, Appl. Phys. Lett. **84**, 3606 (2004).